Reactions of $[NEt_4][10\text{-}endo\text{-}\{Au(PPh_3)\}\text{-}nido\text{-}7,8\text{-}C_2B_9H_9Me_2]$: Carbaborane Cage Transfer from Gold to Iridium *

John C. Jeffery,[a] Paul A. Jelliss[a] and F. Gordon A. Stone[b]
[a] *School of Chemistry, The University, Bristol BS8 1TS, UK*
[b] *Department of Chemistry, Baylor University, Waco, TX, 76798-7348, USA*

The salt $[NEt_4][10\text{-}endo\text{-}\{Au(PPh_3)\}\text{-}nido\text{-}7,8\text{-}C_2B_9H_9Me_2]$ reacts with *trans*-$[IrCl(CO)(PPh_3)_2]$ in thf (tetrahydrofuran), in the presence of $TlBF_4$, to afford the complex $[IrAu(CO)(PPh_3)_2(\eta^5\text{-}7,8\text{-}C_2B_9H_9Me_2)]$. The structure of this product was established by X-ray crystallography. The iridium is co-ordinated on one side by the open pentagonal face of a *nido*-icosahedral $7,8\text{-}C_2B_9H_9Me_2$ group in an η^5 bonding mode, and on the other by the PPh_3 and CO ligands and an $Au(PPh_3)$ fragment [Ir–Au 2.616(2), Au–P 2.251(3) Å, Ir–Au–P 175.8(1)°]. The related compound $[IrAu(CO)_2(PPh_3)(\eta^5\text{-}7,8\text{-}C_2B_9H_9Me_2)]$ is formed in the corresponding reaction using *cis*-$[IrCl(CO)_2(NH_2C_6H_4Me\text{-}4)]$. Small and variable amounts of a metal cluster species $[Ir_2Au_4(\mu\text{-}\sigma:\eta^5\text{-}7,8\text{-}C_2B_9H_8Me_2)(CO)_3(PPh_3)_4][7,8\text{-}C_2B_9H_{10}Me_2]$ are also produced in the latter reaction. Treatment of $[IrCl(PPh_3)_3]$ with $[NEt_4][10\text{-}endo\text{-}\{Au(PPh_3)\}\text{-}nido\text{-}7,8\text{-}C_2B_9H_9Me_2]$ affords the dimetal complex $[IrAuH(\mu\text{-}\sigma:\eta^3\text{-}7,8\text{-}C_2B_9H_8Me_2)(PPh_3)_3]$, the structure of which was determined by X-ray crystallography. The Ir–Au bond [2.739(1) Å] is spanned by a $7,8\text{-}C_2B_9H_8Me_2$ group. The open CCBBB pentagonal ring of the cage is attached to the iridium *via* its three boron atoms, while also being σ bonded to the gold atom through the boron atom in the β site with respect to the two carbons [Au–B 2.200(9) Å]. The gold atom carries a PPh_3 ligand [Au–P 2.320(2) Å, P–Au–Ir 164.6(1)°], and the iridium is co-ordinated by two such groups [Ir–P 2.293 Å (average), P–Ir–P 100.3(1)°] and a hydride ligand transoid to the gold [Ir–H 1.58(9) Å, H–Ir–Au 168(3)°]. The NMR data (^1H, $^{13}C\text{-}\{^1H\}$, $^{31}P\text{-}\{^1H\}$ and $^{11}B\text{-}\{^1H\}$) of the new compounds are reported and discussed in relation to the structures.

We have recently described the synthesis of the salt $[NEt_4][10\text{-}endo\text{-}\{Au(PPh_3)\}\text{-}nido\text{-}7,8\text{-}C_2B_9H_9Me_2]$ **1a**, and have reported its reactions with the rhodium complexes *trans*-$[RhCl(CO)(PPh_3)_2]$, $[Rh_2(\mu\text{-}Cl)_2(CO)_4]$, $[RhCl(PPh_3)_3]$ and $[Rh(cod)(PPh_3)_2][PF_6]$ (cod = cycloocta-1,5-diene).[1] Several mixed-metal compounds containing gold-rhodium bonds were isolated, including the novel species $[exo\text{-}5,10\text{-}\{Rh(PPh_3)_2\}\text{-}5,10\text{-}(\mu\text{-}H)_2\text{-}10\text{-}endo\text{-}\{Au(PPh_3)\}\text{-}nido\text{-}7,8\text{-}C_2B_9H_7Me_2]$ **2** and $[RhAu_2(\mu\text{-}H)(PPh_3)_3(\eta^5\text{-}7,8\text{-}C_2B_9H_9Me_2)]$ **3**. In this paper we describe related reactions between **1a** and iridium complexes which afford products with gold–iridium bonds. Relatively few mixed-metal compounds of this type have been reported,[2,3] and none of those previously described contains carbaborane ligands.

Results and Discussion

In thf (tetrahydrofuran) at room temperature, the compounds **1a** and *trans*-$[IrCl(CO)(PPh_3)_2]$, in the presence of $TlBF_4$ to facilitate removal of chloride as insoluble TlCl, afford $[IrAu(CO)(PPh_3)_2(\eta^5\text{-}7,8\text{-}C_2B_9H_9Me_2)]$ **4a**. This product, formed in high yield (*ca.* 90%), is the iridium analogue of the rhodium complex **4b**, previously prepared either by treating *trans*-$[RhCl(CO)(PPh_3)_2]$ with **1a**,[1] or by treating $[AuCl(PPh_3)]$ with $[NEt_4][Rh(CO)(PPh_3)(\eta^5\text{-}7,8\text{-}C_2B_9H_9Me_2)]$.[4a]

Compound **4a** was characterised by the data given in Tables 1–3, and also by an X-ray diffraction study. The results of the latter are summarised in Table 4 and the structure is shown in Fig. 1. The iridium atom is co-ordinated on one side by the *nido*-$7,8\text{-}C_2B_9H_9Me_2$ cage, in the usual pentahapto fashion for this ligand, and on the other by the CO and PPh_3 groups, and the $Au(PPh_3)$ moiety. Both the latter and the carbonyl group are attached to the iridium in an essentially linear manner [Ir–Au–P(2) 175.8(1), Ir–C(3)–O 177(1)°]. The Ir–Au separation [2.616(2) Å] is comparable with the average of those found for the iridium–gold distances in the cluster compounds $[IrAu_2H(NO_3)(PPh_3)_4][BF_4]$ (2.685 Å), $[IrAu_3(NO_3)(PPh_3)_5][BF_4]$ (2.641 Å) and $[IrAu_4(\mu\text{-}H)_2(PPh_3)_6][BF_4]$ (2.690 Å),[2] but somewhat shorter than that in the dinuclear metal complex $[IrAuH_3(PPh_3)_4][BF_4]$ [2.765(1) Å].[3]

As expected, the IR spectrum of compound **4a** displays a single CO stretching band at 1971 cm^{-1}, to be compared with that seen in the spectrum of **4b** at 1983 cm^{-1}.[4a] In their $^{31}P\text{-}\{^1H\}$ NMR spectra both species show two resonances for the non-equivalent PPh_3 ligands. The signals for **4a** (Table 3) are doublets at δ 11.0 [PIr, *J*(PP) 10] and 37.4 [PAu, *J*(PP) 10 Hz], and those for **4b** doublets at δ 43.9 [PRh, *J*(RhP) 149] and 36.3 [PAu, *J*(RhP) 8 Hz].[1] The $^{13}C\text{-}\{^1H\}$ NMR spectrum of **4a** indicates the non-equivalence of the cage CMe fragments, with resonances at δ 63.9 [*J*(PC) 9] and 63.0 [*J*(PC) 26 Hz] for the *C*Me nuclei, and peaks at δ 33.1 and 29.2 for the C*Me* groups. The $^{13}C\text{-}\{^1H\}$ NMR spectrum of **4b** is similar, except that one of the *C*Me signals is broad, the $^{31}P\text{–}^{13}C$ coupling being unresolved.[1] The iridium and rhodium atoms in **4a** and **4b** are chiral centres, and thus the cage CMe groups would be non-equivalent even if the molecules exhibited dynamic behaviour. The latter would involve rotation about an axis through the metal atoms and the centroids of the ligating pentagonal faces of the *nido*-$7,8\text{-}C_2B_9H_9Me_2$ fragments. However, the observation in the $^{13}C\text{-}\{^1H\}$ NMR spectrum of **4a** of two different $^{31}P\text{–}^{13}C$ couplings (9 and 26 Hz) on the two *C*Me resonances establishes that the molecule is probably static on the NMR time-scale, otherwise the two *J*(PC) values would be averaged to a similar magnitude. Moreover, from crystal structure data (Table 4) it is

* *Supplementary data available:* see Instructions for Authors, *J. Chem. Soc., Dalton Trans.*, 1993, Issue 1, pp. xxiii–xxviii.

Table 1 Analytical and physical data for the complexes

Compound	Colour	Yield (%)	ν_{max}(CO)[a]/cm^{-1}	Analysis (%)[b] C	H
4a $[IrAu(CO)(PPh_3)_2(\eta^5\text{-}7,8\text{-}C_2B_9H_9Me_2)]$	Yellow	89	1971vs	45.0 (44.7)	4.1 (4.1)
4c $[IrAu(CO)_2(PPh_3)(\eta^5\text{-}7,8\text{-}C_2B_9H_9Me_2)]$	Pale orange	67[c]	2051vs, 2002s	33.1 (33.2)	3.7 (3.5)
6 $[Ir_2Au_4(\mu\text{-}\sigma\text{:}\eta^5\text{-}7,8\text{-}C_2B_9H_8Me_2)(CO)_3(PPh_3)_4][7,8\text{-}C_2B_9H_{10}Me_2]$	Bright yellow	17[d]	2043s, 1996s, 1956m	37.3 (38.0)	3.3 (3.5)
7 $[NEt_4][Ir(CO)_2(\eta^5\text{-}7,8\text{-}C_2B_9H_9Me_2)]$	Pale brown	57	2001vs, 1930m	[e] 31.6 (31.2)	5.6 (6.6)
8 $[IrAuH(\mu\text{-}\sigma\text{:}\eta^3\text{-}7,8\text{-}C_2B_9H_8Me_2)(PPh_3)_3]$	Bright orange	88		51.9 (52.1)	4.4 (4.5)
9a $[IrAu(PPh_3)_3(\eta^5\text{-}7,8\text{-}C_2B_9H_{11})]$	Yellow	77		51.5 (51.4)	4.8 (4.3)

[a] Measured in CH_2Cl_2; medium-intensity broad bands observed at *ca.* 2550 cm^{-1} in the spectra of all the compounds are due to B–H absorptions. [b] Calculated values are given in parentheses. [c] Yield is *ca.* 65% when prepared from compounds **7** and $[AuCl(PPh_3)]$. [d] Yield is variable; from negligible to *ca.* 15% maximum. [e] N, 2.7 (2.6)%.

Table 2 Hydrogen-1 and carbon-13 NMR data[a] for the complexes

Compound	^{1}H (δ)[b]	^{13}C (δ)[c]
4a	1.96, 2.38 (s × 2, 6 H, CMe), 7.15–7.75 (m, 30 H, Ph)	179.4 [d, CO, *J*(PC) 15], 134.9–128.1 (Ph), 63.9 [d, *C*Me, *J*(PC) 9], 63.0 [d, *C*Me, *J*(PC) 26], 33.1, 29.2 (s × 2, C*Me*)
4c	2.62 (s, 6 H, CMe), 7.52–7.61 (m, 15 H, Ph)	172.9 (s, CO), 134.5 [d, C^2(Ph), *J*(PC) 14], 132.2 [C^4(Ph)], 130.3 [d, C^1(Ph), *J*(PC) 57], 129.7 [d, C^3(Ph), *J*(PC) 12], 71.3 (br, *C*Me), 32.9 (C*Me*)
6[d]	−2.6 (br, 1 H, H_{endo}), 1.37* (s, 6 H, CMe), 2.63 (s, 6 H, CMe), 7.08–7.38 (m, 60 H, Ph)	186.8 (s, CO × 1), 173.2 (s, CO × 2), 134.2–129.0 (Ph), 62.3 (br, *C*Me), 57.5* (vbr, *C*Me), 32.1 (C*Me*), 21.7* (C*Me*)
7	1.34 [t of t, 12 H, CH_2Me, *J*(HH) 7, *J*(NH) 2], 2.45 (s, 6 H, CMe), 3.20 [q, 8 H, NCH_2, *J*(HH) 7]	182.0 (s, CO), 59.9 (br, *C*Me), 53.2 (NCH_2), 32.7 (C*Me*), 7.9 (CH_2Me)
8	−15.21 [d of t, 1 H, IrH, *J*(PH) 22 and 22], 0.91 (s, 6 H, CMe), 6.88–7.52 (m, 45 H, Ph)	136.7 [d, C^1(IrPPh), *J*(PC) 50], 134.9 [d, C^2(IrPPh), *J*(PC) 10], 134.7 [d, C^2(AuPPh), *J*(PC) 15], 131.6 [d, C^1(AuPPh), *J*(PC) 44], 131.5 [C^4(AuPPh)], 129.5 [d, C^3(AuPPh), *J*(PC) 11], 129.4 [C^4(IrPPh)], 127.4 [d, C^3(IrPPh), *J*(PC) 9], 76.3 (br, *C*Me), 20.3 (C*Me*)
9a	2.37 (s, br, 2 H, CH), 6.93–7.62 (m, 45 H, Ph)	[e] 136.7 [AXX', C^1(IrPPh), *N* 51], [e] 134.6 [AXX', C^2(IrPPh), *N* 10], 134.5 [d, C^2(AuPPh), *J*(PC) 13], 132.5 [d, C^1(AuPPh), *J*(PC) 50], 131.4 [C^4(AuPPh)], 129.5 [C^4(IrPPh)], 129.4 [d, C^3(AuPPh), *J*(PC) 10], [e] 127.6 [AXX', C^3(IrPPh), *N* 9], 40.8 (CH)

[a] Chemical shifts δ in ppm, coupling constants in Hz, measurements at room temperature in CD_2Cl_2. [b] Proton resonances for terminal BH groups occur as broad unresolved signals in the range δ *ca.* −2 to +3. [c] Hydrogen-1 decoupled chemical shifts are positive to high frequency of $SiMe_4$. Measurements in CD_2Cl_2–CH_2Cl_2. [d] Peaks asterisked are due to the CMe group of the anion $[7,8\text{-}C_2B_9H_{10}Me_2]^-$. [e] Insufficient resolution prevents full analysis of coupling constants; $N = |J(AX) + J(AX')|$.

Table 3 Boron-11 and phosphorus-31 NMR data[a] for the complexes

Compound	^{11}B (δ)[b]	^{31}P (δ)[c]
4a	−4.6 (br, 1 B), −8.5 (br, 1 B), −9.7 (br, 2 B), −11.2 (br, 2 B), −15.3 (br, 2 B), −18.8 (br, 1 B)	37.4 [d, PAu, *J*(PP) 10], 11.0 [d, PIr, *J*(PP) 10]
4c	−0.1 (br, 1 B), −9.3 (br, 1 B), −11.2 (br, 4 B), −15.1 (br, 3 B)	42.3 (s, PAu)
6[d]	38.3 (br, 1 B, BIr), −3.2 (br, 1 B), −9.2 (vbr, 6 B), −11.2* (br, 3 B), −12.9 (br, 1 B), −20.4* (br, 4 B), −36.8* (br, 1 B), −38.9* (br, 1 B)	51.2 (s, PAu)
7	−10.5 (br, 2 B), −14.5 (br, 4 B), −16.9 (br, 1 B), −18.0 (br, 2 B)	
8	66.5 (br, 1 B, BAu), −0.5 (br, 2 B), −5.7 (br, 2 B), −11.9 (br, 1 B), −20.0 (br, 1 B), −39.1 (br, 2 B)	58.3 (br, PAu), 18.8 (br, PIr)
9a	−4.3 (br, 1 B), −7.5 (br, 1 B), −13.7 (br, 4 B), −24.9 (br, 3 B)	38.6 [t, PAu, *J*(PP) 12], 13.9 [d, PIr, *J*(PP) 12]

[a] Chemical shifts δ in ppm, coupling constants in Hz, measurements at room temperature in CD_2Cl_2. [b] Hydrogen-1 decoupled, chemical shifts are positive to high frequency of BF_3·Et_2O (external). [c] Hydrogen-1 decoupled, chemical shifts are positive to high frequency of 85% H_3PO_4 (external). [d] Signals asterisked are due to the anion $[7,8\text{-}C_2B_9H_{10}Me_2]^-$.

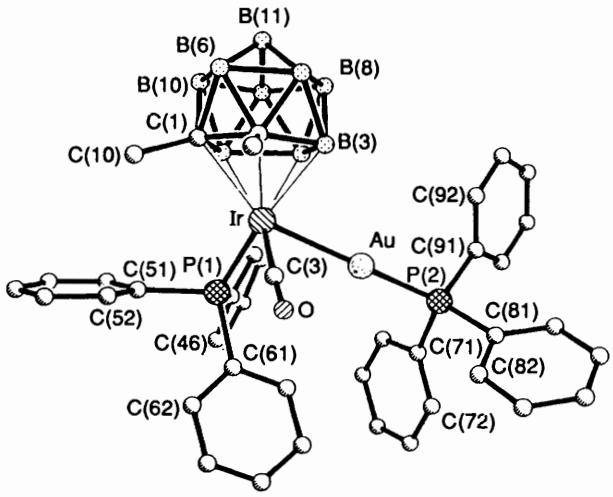

Fig. 1 Molecular structure of $[IrAu(CO)(PPh_3)_2(\eta^5\text{-}7,8\text{-}C_2B_9H_9Me_2)]$ **4a**, showing the crystallographic labelling scheme

seen that angles P(1)–Ir–C(1) and P(1)–Ir–C(2) are 111.8(2) and 151.2(3)°, respectively. Since P(1) is transoid to C(2) we assign the larger coupling (26 Hz) to *J*[P(1)C(2)] (Fig. 1). A similar argument can be applied to the rhodium–gold compound **4b** where the PC coupling constants are correspondingly different (< 2 and 25 Hz).

During the preparation of compound **4a** the formation of a minor product in trace quantities was observed. This species was not identified in the present study, but was subsequently

Table 4 Selected internuclear distances (Å) and angles (°) for the complex $[IrAu(CO)(PPh_3)_2(\eta^5\text{-}7,8\text{-}C_2B_9H_9Me_2)]$ **4a**

Ir–Au	2.616(2)	Ir–P(1)	2.306(3)	Ir–C(1)	2.36(1)	Ir–C(2)	2.28(1)
Ir–B(3)	2.24(1)	Ir–B(4)	2.27(1)	Ir–B(5)	2.25(1)	Ir–C(3)	1.87(1)
Au–P(2)	2.251(3)	C(1)–C(2)	1.66(1)	C(1)–B(5)	1.70(2)	C(1)–B(6)	1.74(2)
C(1)–B(10)	1.70(2)	C(1)–C(10)	1.53(1)	C(2)–B(3)	1.73(2)	C(2)–B(6)	1.77(2)
C(2)–B(7)	1.71(2)	C(2)–C(20)	1.53(1)	B(3)–B(4)	1.82(2)	B(3)–B(7)	1.78(2)
B(3)–B(8)	1.79(2)	B(3)–H(3)	0.9(1)	B(4)–B(5)	1.84(2)	B(4)–B(8)	1.78(2)
B(4)–B(9)	1.80(2)	B(4)–H(4)	1.0(1)	B(5)–B(9)	1.80(2)	B(5)–B(10)	1.81(2)
B(5)–H(5)	1.2(1)	B(6)–B(7)	1.77(2)	B(6)–B(10)	1.72(2)	B(6)–B(11)	1.75(2)
B(6)–H(6)	1.1(1)	B(7)–B(8)	1.75(2)	B(7)–B(11)	1.78(2)	B(7)–H(7)	1.0(1)
B(8)–B(9)	1.76(2)	B(8)–B(11)	1.76(2)	B(8)–H(8)	1.2(1)	B(9)–B(10)	1.76(2)
B(9)–B(11)	1.75(2)	B(9)–H(9)	1.0(1)	B(10)–B(11)	1.73(2)	B(10)–H(10)	1.0(1)
B(11)–H(11)	1.2(1)	C(3)–O	1.11(1)				

Au–Ir–P(1)	86.9(1)	Au–Ir–C(1)	151.2(2)	P(1)–Ir–C(1)	111.8(2)
Au–Ir–C(2)	121.9(2)	P(1)–Ir–C(2)	151.2(3)	C(1)–Ir–C(2)	41.9(3)
Au–Ir–B(3)	79.5(3)	P(1)–Ir–B(3)	158.3(3)	C(1)–Ir–B(3)	75.6(4)
C(2)–Ir–B(3)	45.0(4)	Au–Ir–B(4)	75.6(3)	P(1)–Ir–B(4)	112.7(3)
C(1)–Ir–B(4)	76.9(4)	C(2)–Ir–B(4)	77.1(4)	B(3)–Ir–B(4)	47.5(4)
Au–Ir–B(5)	117.8(3)	P(1)–Ir–B(5)	92.4(3)	C(1)–Ir–B(5)	43.2(4)
C(2)–Ir–B(5)	74.0(4)	B(3)–Ir–B(5)	79.3(5)	B(4)–Ir–B(5)	47.9(4)
Au–Ir–C(3)	81.1(3)	P(1)–Ir–C(3)	88.0(3)	C(1)–Ir–C(3)	119.7(4)
C(2)–Ir–C(3)	97.0(4)	B(3)–Ir–C(3)	106.4(5)	B(4)–Ir–C(3)	147.5(4)
B(5)–Ir–C(3)	161.1(4)	Ir–Au–P(2)	175.8(1)	Ir–C(1)–C(2)	66.5(5)
Ir–C(1)–B(5)	65.1(5)	Ir–C(1)–C(10)	112.0(7)	Ir–C(2)–C(1)	71.6(5)
Ir–C(2)–B(3)	66.2(5)	Ir–C(2)–C(20)	111.4(7)	Ir–B(3)–C(2)	68.8(5)
Ir–B(3)–B(4)	67.3(5)	Ir–B(3)–H(3)	114(7)	Ir–B(4)–B(3)	65.2(5)
Ir–B(4)–B(5)	65.5(5)	Ir–B(4)–H(4)	130(6)	Ir–B(5)–C(1)	71.7(5)
Ir–B(5)–B(4)	66.6(5)	Ir–B(5)–H(5)	118(5)	Ir–C(3)–O	177(1)

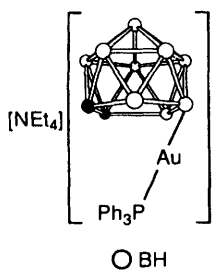

○ BH

● CMe

1a CMe
1b CH

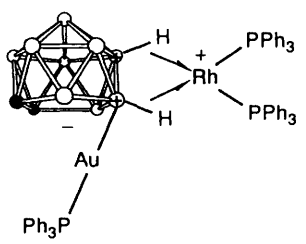

2 ● CMe ○ BH ⊕ B

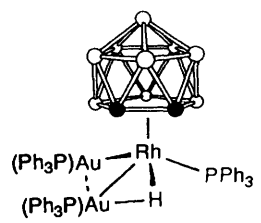

3 ● CMe ○ BH

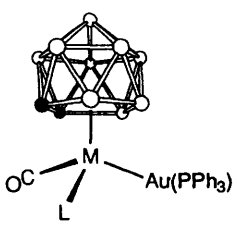

● CMe ○ BH

	M	L
4a	Ir	PPh_3
4b	Rh	PPh_3
4c	Ir	CO
4d	Rh	CO

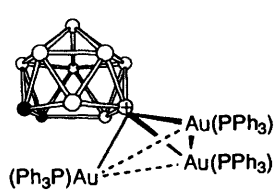

5 ● CMe ○ BH ⊕ B

characterised by X-ray crystallography as the novel trigold compound **5**.[5] It may be isolated in good yield from reactions between **1a** and $[AuCl(PPh_3)]$ under suitable conditions. Its mode of formation as a by-product in the synthesis of **4a** is obscure at the present time.

The reaction between compounds **1a** and *cis*-$[IrCl(CO)_2(NH_2C_6H_4Me\text{-}4)]$, in the presence of $TlBF_4$, was next investigated. Column chromatography on alumina of the reaction mixture separated the dimetal compound $[IrAu(CO)_2(PPh_3)(\eta^5\text{-}7,8\text{-}C_2B_9H_9Me_2)]$ **4c** from a hexanuclear species $[Ir_2Au_4(\mu\text{-}\sigma\text{:}\eta^5\text{-}7,8\text{-}C_2B_9H_8Me_2)(CO)_3(PPh_3)_4][7,8\text{-}C_2B_9H_{10}Me_2]$ **6**. In some reactions the latter was formed in trace amounts, and the best yields were no higher than *ca.* 15%. Persistent efforts were made to grow crystals of **6** for a structurally definitive X-ray

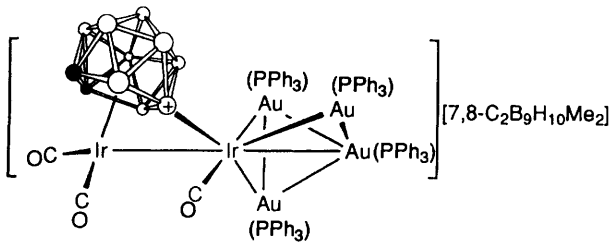

6 ● CMe ○ BH ⊕ B

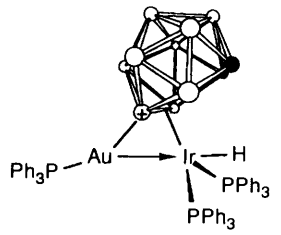

8 ● CMe ○ BH ⊕ B

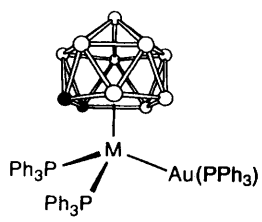

○ BH

	M	●
9a	Ir	CH
9b	Rh	CH
9c	Rh	CMe

diffraction study. Although good-quality crystals were not obtained, data from one crystal established the metal core structure depicted.

In agreement with the presence in compound **6** of the three carbonyl ligands, three CO stretching bands were observed in the IR spectrum (Table 1). The molecule shows facile dynamic behaviour in solution, as evidenced by the observation of only one resonance (δ 51.2) for the $Au(PPh_3)$ groups in the $^{31}P-\{^1H\}$ NMR spectrum even at −80 °C. In the $^{13}C-\{^1H\}$ NMR spectrum (Table 2) there are two CO resonances at δ 186.8 and 173.2 of relative intensity 1 : 2, respectively. We assign the former deshielded signal to the carbonyl ligand attached to the iridium linked to the gold atoms, formally carrying a positive charge and having a 16-electron valence shell, and the latter peak to the $Ir(CO)_2$ group. This iridium centre formally has an 18-electron valence shell.

Both the ^1H and $^{13}C-\{^1H\}$ NMR spectra (Table 2) of compound **6** confirm the presence of two carbaborane cages, one of which occurs as the counter anion $[7,8-C_2B_9H_{10}Me_2]^-$. In the ^1H NMR spectrum a diagnostic resonance is seen at δ −2.6 for the *endo*-H proton present in the open face of the anion. The $^{11}B-\{^1H\}$ NMR spectrum, data from which are listed in Table 3, was also informative. Peaks due to two C_2B_9 cage systems are observed. Moreover, a deshielded signal at δ 38.3 is diagnostic for the B–Ir σ bond present in the cation of **6**. Resonances for BIr groups have been observed previously in the range δ 23.2–45.0.[6]

Compound **4c**, the principal product of the reaction between **1a** and *cis*-$[IrCl(CO)_2(NH_2C_6H_4Me\text{-}4)]$, was characterised by the data summarised in Tables 1–3. It is the iridium analogue of the previously prepared rhodium compound **4d**. The latter has been obtained by two methods, either by treating $[AuCl(PPh_3)]$ with $[NEt_4][Rh(CO)_2(\eta^5\text{-}7,8\text{-}C_2B_9H_9Me_2)]$,[4b] or from the reaction between the salt **1a** and $[Rh_2(\mu\text{-}Cl)_2(CO)_4]$.[1] In the present work we have prepared the salt $[NEt_4][Ir(CO)_2(\eta^5\text{-}7,8\text{-}C_2B_9H_9Me_2)]$ **7**, and have treated this reagent with $[AuCl(PPh_3)]$ in an alternative synthesis for **4c**. Data characterising the new complex **7** are listed in Tables 1–3.

The reaction between compounds **1a** and $[RhCl(PPh_3)_3]$ affords the *exo-nido* species **2**.[1] This result prompted a study of the corresponding reaction between **1a** and $[IrCl(PPh_3)_3]$. The product of the latter reaction is the complex $[IrAuH(\mu\text{-}\sigma:\eta^3\text{-}7,8\text{-}C_2B_9H_8Me_2)(PPh_3)_3]$ **8**, formed in high yield (Table 1). The nature of **8** was not established until after an X-ray diffraction study had been carried out, the results of which are summarised in Table 5, the structure being shown in Fig. 2.

The Au–Ir bond [2.739(1) Å] is appreciably longer than that in compound **4a** [2.616(2) Å], being comparable with that [2.765(1) Å] in the cation $[IrAuH_3(PPh_3)_4]^+$ mentioned earlier.[3] The metal–metal bond in **8** is bridged by a $7,8\text{-}C_2B_9H_8Me_2$ cage system in such a manner that it is σ bonded to the gold atom [Au–B(4) 2.200(9) Å], while being η^3 co-ordinated to the iridium [Ir–B(3) 2.331(9), Ir–B(4) 2.03(1), Ir–B(5) 2.42(1) Å]. This trihapto bonding mode of the cage to the iridium is best shown in Fig. 3, which also serves to depict the bonding of the phosphorus atoms of the three PPh_3 groups [P(3)–Au–Ir 164.6(1), P(3)–Au–B(4) 148.5(3), P(1)–Ir–P(2) 100.3(1), P(1)–Ir–Au 92.3(1), P(2)–Ir–Au 101.7(1)°].

A significant feature revealed by the X-ray diffraction study, in addition to the η^3 co-ordination of the cage, is the non-planarity of the C_2B_3 face of the ligand. The metal slippage and cage–face folding can be quantified by the slip (Δ) and fold (φ and θ) distortion parameters,[7] and these are listed in Table 6. Also included are similar data for compound **4a**, where the cage is η^5 co-ordinated to iridium, and for compound **2**[1] where the gold atom is essentially σ bonded to the boron atom β to the carbons in the face of the cage. The η^3 interaction with the iridium atom in **8** has caused a substantial folding of the C_2B_3 face of the cage about the B(3)···B(5) vector such that the plane defined by B(3)B(4)B(5) is inclined relative to the plane B(6)B(7)B(8)B(9)B(10) by φ = 9.9° and the B(5)C(1)C(2)B(3) plane is inclined relative to the latter by θ = 6.8°. This electronic effect combines with the demands of the B(4)–Au→Ir interaction to force the iridium atom to slip from the perpendicular through the centroid of the non-bonded B_5 pentagonal belt by a considerable distance, Δ = 1.24 Å. This is further than the slippage of the σ-bonded *endo*-gold atom in the structure[1] of complex **2** where Δ = 1.05 Å (φ = 6.1 and θ = 2.2°). These data may be compared with those for compound **4a** where cage–face folding is small (both φ and θ = 2.2°) and the iridium atom can be considered as non-slipped (Δ = 0.17 Å). The distortion from planarity of the C_2B_3 girdle in compound **8** is also reflected in the mean deviation of the atoms C(1)C(2)-B(3)B(4)B(5) from a least-squares plane [$\delta(C_2B_3)$ = 0.089 Å] while the non-co-ordinated belt B(6)B(7)B(8)B(9)B(10) is also slightly distorted [$\delta(B_5)$ = 0.032 Å], presumably as a

Table 5 Selected internuclear distances (Å) and angles (°) for the complex $[IrAuH(\mu\text{-}\sigma:\eta^3\text{-}7,8\text{-}C_2B_9H_8Me_2)(PPh_3)_3]$ **8**

Ir–H(001)	1.58(9)	Ir–Au	2.739(1)	Ir–P(1)	2.295(2)	Ir–P(2)	2.291(2)
Ir–B(3)	2.331(9)	Ir–B(4)	2.03(1)	Ir–B(5)	2.42(1)	Au–P(3)	2.320(2)
Au–B(4)	2.200(9)	C(1)–C(2)	1.51(1)	C(1)–C(10)	1.53(1)	C(1)–B(5)	1.71(1)
C(1)–B(6)	1.71(1)	C(1)–B(10)	1.67(1)	C(2)–C(20)	1.50(1)	C(2)–B(3)	1.74(1)
C(2)–B(6)	1.73(1)	C(2)–B(7)	1.68(1)	B(3)–B(4)	1.81(1)	B(3)–B(7)	1.83(1)
B(3)–B(8)	1.87(2)	B(3)–H(3)	1.18(9)	B(4)–B(5)	1.80(1)	B(4)–B(8)	1.72(1)
B(4)–B(9)	1.76(1)	B(5)–B(9)	1.89(2)	B(5)–B(10)	1.82(2)	B(5)–H(5)	1.10(9)
B(6)–B(7)	1.76(2)	B(6)–B(10)	1.74(2)	B(6)–B(11)	1.76(2)	B(6)–H(6)	1.16(9)
B(7)–B(8)	1.76(2)	B(7)–B(11)	1.77(2)	B(7)–H(7)	1.11(9)	B(8)–B(9)	1.77(2)
B(8)–B(11)	1.75(2)	B(8)–H(8)	1.15(9)	B(9)–B(10)	1.76(2)	B(9)–B(11)	1.74(2)
B(9)–H(9)	1.04(9)	B(10)–B(11)	1.79(2)	B(10)–H(10)	1.2(1)	B(11)–H(11)	1.0(1)

H(001)–Ir–Au	168(3)	H(001)–Ir–P(1)	83(3)	Au–Ir–P(1)	92.3(1)
H(001)–Ir–P(2)	90(3)	Au–Ir–P(2)	101.7(1)	P(1)–Ir–P(2)	100.3(1)
H(001)–Ir–B(3)	91(3)	Au–Ir–B(3)	91.8(3)	P(1)–Ir–B(3)	169.5(3)
P(2)–Ir–B(3)	88.4(3)	H(001)–Ir–B(4)	123(3)	Au–Ir–B(4)	52.4(3)
P(1)–Ir–B(4)	129.0(3)	P(2)–Ir–B(4)	120.1(3)	B(3)–Ir–B(4)	48.4(4)
H(001)–Ir–B(5)	87(3)	Au–Ir–B(5)	82.7(3)	P(1)–Ir–B(5)	100.8(3)
P(2)–Ir–B(5)	158.2(3)	B(3)–Ir–B(5)	70.1(4)	B(4)–Ir–B(5)	46.6(4)
Ir–Au–P(3)	164.6(1)	Ir–Au–B(4)	46.9(3)	P(3)–Au–B(4)	148.5(3)
Ir–B(3)–C(2)	101.1(5)	Ir–B(3)–B(4)	56.9(4)	Ir–B(3)–H(3)	108(4)
Ir–B(4)–Au	80.7(3)	Ir–B(4)–B(3)	74.7(5)	Au–B(4)–B(3)	131.1(6)
Ir–B(4)–B(5)	78.5(5)	Au–B(4)–B(5)	117.2(6)	Au–B(4)–B(8)	125.0(6)
Au–B(4)–B(9)	115.6(6)	Ir–B(5)–C(1)	100.0(6)	Ir–B(5)–B(4)	54.9(4)
Ir–B(5)–H(5)	101(5)				

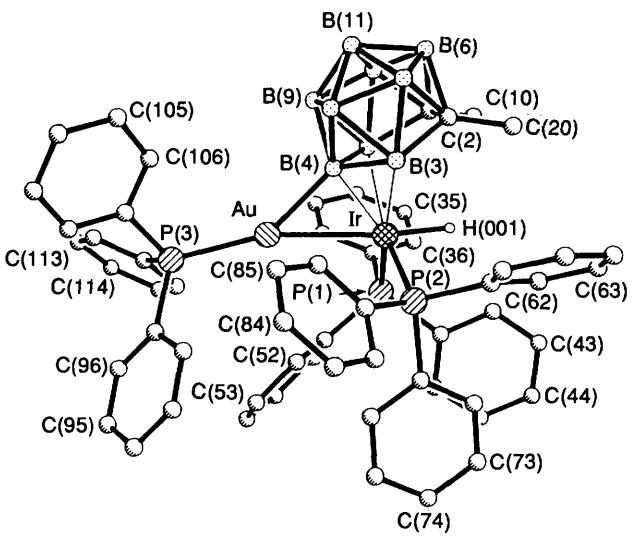

Fig. 2 Molecular structure of $[IrAuH(\mu\text{-}\sigma:\eta^3\text{-}7,8\text{-}C_2B_9H_8Me_2)(PPh_3)_3]$ **8**, showing the crystallographic labelling scheme

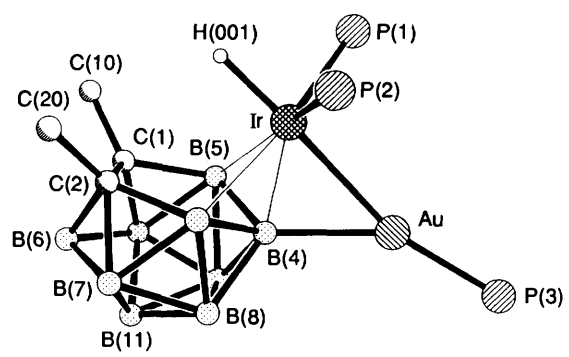

Fig. 3 Part of the molecular structure of $[IrAuH(\mu\text{-}\sigma:\eta^3\text{-}7,8\text{-}C_2B_9H_8Me_2)(PPh_3)_3]$ **8**, highlighting the η^3 co-ordination of the carbaborane cage

steric consequence of the severely buckled C_2B_3 belt below it.

The iridium atom carries a hydride ligand [Ir–H(001) 1.58(9) Å], located in a final electron-density difference map, with its presence confirmed by the ^1H NMR spectrum, discussed below. The site of H(001), transoid to the Au–Ir bond [H(001)–Ir–Au 168(3)°], results in the iridium atom being in an approximately octahedral environment if the B(3)B(4)B(5) fragment is taken as occupying two co-ordination sites, as is usual for η^3-allylic systems.

Table 6 Slip and fold distortion parameters[a] for the systems AuC_2B_9 in compound **2**, and IrC_2B_9 in compounds **4a** and **8**

Compound	Δ/Å	φ/°	θ/°	$\delta(C_2B_3)^b$/Å	$\delta(B_5)^c$/Å
2[d]	1.05	6.1	2.2	0.040	0.013
4a	0.17	2.2	2.2	0.022	0.013
8	1.24	9.9	6.8	0.089	0.032

[a] The slip and fold distortion parameters Δ, φ and θ are fully defined and illustrated in ref. 7. [b] Mean deviation of the atoms of the C_2B_3 face of the cage from a least-squares plane. [c] Similar calculation for the non-co-ordinating B_5 pentagonal belt. [d] Ref. 1.

The NMR data for compound **8** are in agreement with the structure established by X-ray diffraction. The ^1H spectrum (Table 2) has a resonance for the hydride ligand at δ −15.21 which appears as a doublet of triplets [*J*(PH) 22 and 22 Hz]. The molecule has a plane of symmetry through the atoms Au, B(4) and Ir, and the midpoint of the C(1)–C(2) connectivity. Consequently, the cage CMe groups are equivalent giving rise to one resonance for these groups in the ^1H NMR spectrum (δ 0.91) and two peaks in the $^{13}C\text{-}\{^1H\}$ NMR spectrum [δ 76.3 (*C*Me) and 20.3 (C*Me*)]. A deshielded signal in the $^{11}B\text{-}\{^1H\}$ NMR spectrum at δ 66.5, with an intensity corresponding to one boron nucleus, is readily assigned to the BAu group. This signal remains a singlet in a fully coupled ^{11}B spectrum indicating that it is not due to a BH group. The $^{31}P\text{-}\{^1H\}$ NMR spectrum shows two signals arising from the inequivalent PPh_3 groups [δ 58.3 (PAu) and 18.8 (PIr)] which are both broadened (mean peak width at half height 63 Hz) due to the effect of quadrupolar (^{11}B and to a lesser extent ^{197}Au) nuclei and unresolved ^{31}P–^{31}P coupling. The resonance for the $Au(PPh_3)$ group of compound **8** is appreciably more deshielded than those in the spectra of **4a** or **4c** (δ 37.4 and 42.3, respectively), an effect perhaps due to the different nature of the Ir–Au bonds in the two species. In **8** an Au→Ir donor bond is invoked to give the iridium atom a filled valence shell, assuming a two-electron donor borallylic interaction and the usual contributions from

the H and PPh_3 groups. The phosphorus atoms of the $Ir(PPh_3)_2$ group lie on either side of the plane of symmetry, mentioned above, thereby giving rise to one resonance for these nuclei.

Although assigned formally as a borallylic system, a detailed structural analysis[8] of the compound $[IrH(CO)(PPh_3)_2(B_3H_7)]$ suggested that the B_3 unit was bound to the iridium atom chiefly *via* three direct iridium–boron two-electron bonds rather than in a π-allylic fashion (Fig. 4). The basis for suggesting the former mode was that the two outer boron atoms of the B_3H_7 ligand were each *trans* to a phosphorus atom of the *cis*-PPh_3 groups and that these two outer Ir–B bonds lay coplanar with the Ir–P bonds (structure **I**). Structure **II**, where the two B–B vectors are shown *trans* to the phosphorus atoms, would have been expected if the co-ordination had been genuinely allylic. The C_2B_9 cage in compound **8** displays a similarity to this sub-icosahedral fragment (structure **I**, Fig. 4) in its disposition of the boron atoms B(3)B(4)B(5) with respect to the phosphorus atoms P(1) and P(2). This may, however, be a function of the constraint imposed by the β-B–Au–Ir interaction which might cause such a displacement of the co-ordinating B_3 unit in compound **8** so as to render the expected allylic bonding position impossible.

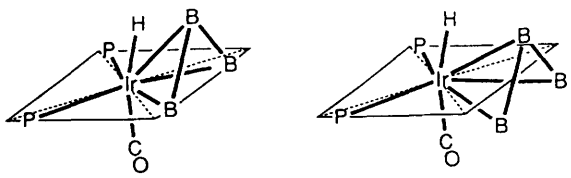

Fig. 4 Two-centre two-electron bonding *versus* borallylic bonding in the complex $[IrH(CO)(PPh_3)_2(B_3H_7)]$. **I**, Observed bonding of B_3H_7 *via* direct Ir–B bonds; **II**, expected bonding position for borallylic B_3H_7

In contrast with the formation of compound **8** from the reaction between **1a** and $[IrCl(PPh_3)_3]$, the iridium reagent reacts with **1b** to give $[IrAu(PPh_3)_3(\eta^5\text{-}7,8\text{-}C_2B_9H_{11})]$ **9a**. The latter was characterised in the usual manner (Tables 1–3). The rhodium analogue **9b** has been prepared by treating $[RhCl(PPh_3)_3]$ with **1b**.[1] As already noted, the reaction between $[RhCl(PPh_3)_3]$ and **1a** afforded the *exo-nido* species **2**. These results show that the nature of the products obtained in these reactions depends critically on whether the reagents **1** contain $7,8\text{-}C_2B_9H_{11}$ or $7,8\text{-}C_2B_9H_9Me_2$ groups.

The syntheses of the iridium–gold complexes **4a**, **4c** and **9a** by employing the reagents **1** involves transfer of the carbaborane cage from being σ bonded to gold to becoming, in the products, pentahapto co-ordinated to iridium. As described previously,[1] the preparation of the rhodium–gold compounds **3**, **4b**, **4d** and

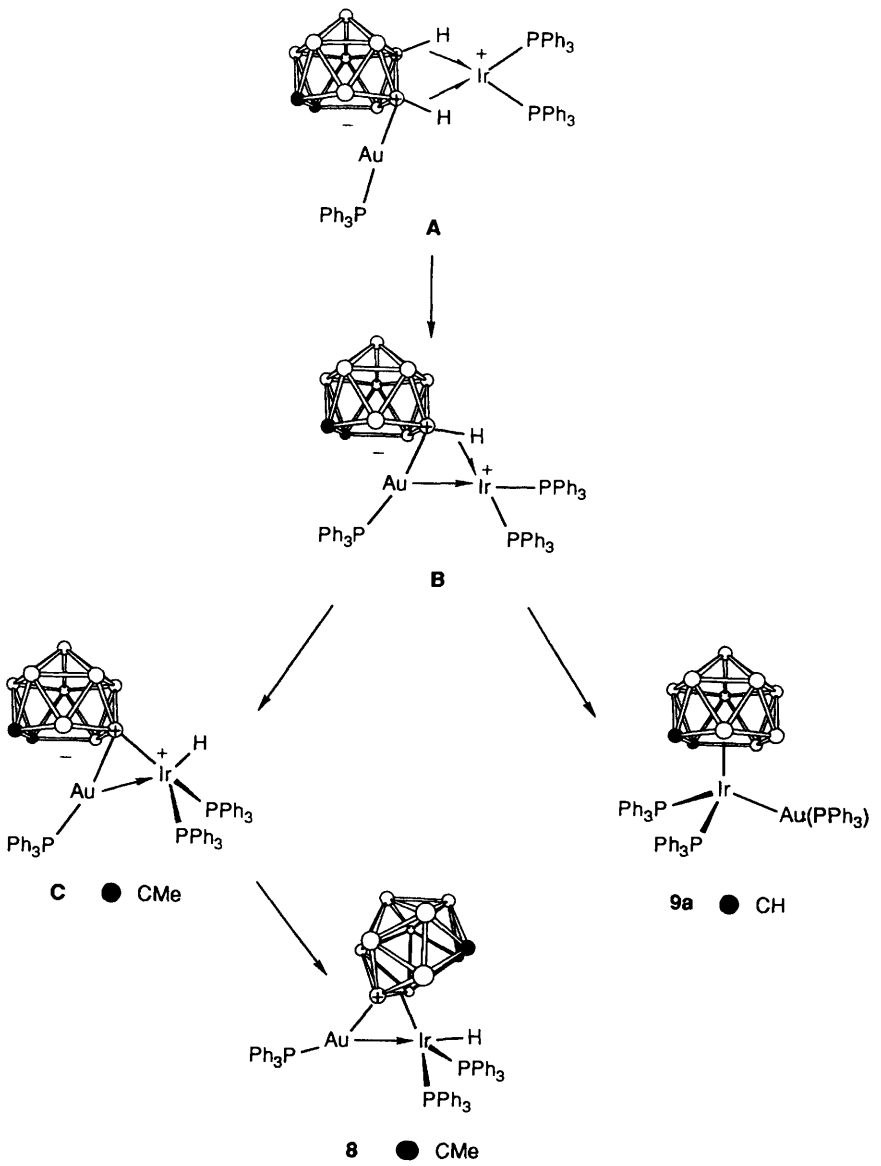

Scheme 1 Proposed mechanisms for cage transfer in the formation of compounds **8** and **9a**. ● = CMe or CH in intermediates **A** and **B**

9b, from the salts **1** and rhodium precursors, also occurs with complete transfer of the cage from gold to rhodium. An exception is the formation of the complex **2** from the reaction between **1a** and $[RhCl(PPh_3)_3]$. In CH_2Cl_2 solutions, however, complex **2** exists in equilibrium with a small amount of its isomer **9c**.[1] Scheme 1 illustrates the possible pathway of cage transfer in formation of the iridium–gold compounds **8** and **9a**. It is proposed that the cage-transfer reactions proceed *via* an intermediate **A** structurally akin to the rhodium complex **2**. Reactions leading to complete transfer of the cage, such as in the formation of **9a**, may then proceed with generation of the intermediate **B**. The product **9a** is then produced from **B** by lifting the B–H→Ir interaction and rotating the carbaborane cage above the metal–metal axis, so that it η^5 ligates the iridium and loses contact with the gold atom. This mechanism could account for the formation of all compounds of type $[MAuL_2(PPh_3)(\eta^5\text{-}7,8\text{-}C_2B_9H_9R_2)]$ (M = Rh or Ir, L = CO or PPh_3, R = Me or H). However, as described above, the reaction between **1a** and $[IrCl(PPh_3)_3]$ yielded **8** as the final product, rather than a complex with structure **A** or one structurally akin to **9a**. Although an iridium complex **A** similar to **2** may form initially in the pathway to **8**, the propensity with which iridium inserts into cage B–H bonds, activated by the presence of CMe groups,[6] may render such a species kinetically unstable leading us to invoke the 'oxidative-addition' intermediate **C** on the route to the observed product **8**. The latter could form from **C** by rotation of the carbaborane cage above the iridium–gold bond. The results discussed here further substantiate the ability of CMe groups to activate B–H bonds which are β to the carbons in the open-pentagonal C_2B_3 faces of $7,8\text{-}C_2B_9H_9Me_2$ ligands.

Experimental

General experimental techniques and instrumentation were described previously, as was the preparation of the salt $[NEt_4][10\text{-}endo\text{-}\{Au(PPh_3)\}\text{-}nido\text{-}7,8\text{-}C_2B_9H_9Me_2]$.[1] The salt $[NEt_4][10\text{-}endo\text{-}\{Au(PPh_3)\}\text{-}nido\text{-}7,8\text{-}C_2B_9H_{11}]$ **1b** was prepared by the method used to obtain the $[N(CH_2Ph)Me_3]^+$ analogue.[9] The reagents *trans*-$[IrCl(CO)(PPh_3)_2]$,[10] *cis*-$[IrCl(CO)_2(NH_2C_6H_4Me\text{-}4)]$,[11] $[AuCl(PPh_3)]$[12] and $[IrCl(PPh_3)_3]$[13] were made by procedures previously described.

Reactions of the Reagents $[NEt_4][10\text{-}endo\text{-}\{Au(PPh_3)\}\text{-}nido\text{-}7,8\text{-}C_2B_9H_9R_2]$ (R = Me *or* H).—(*i*) A mixture of compound **1a** (0.20 g, 0.27 mmol), *trans*-$[IrCl(CO)(PPh_3)_2]$ (0.22 g, 0.28 mmol), and $TlBF_4$ (0.09 g, 0.31 mmol) was stirred at room temperature in thf (20 cm^3) for 16 h, after which time there was no further change in the IR spectrum. Solvent was removed *in vacuo* and CH_2Cl_2 (30 cm^3) was added to the residue. The resulting suspension was filtered through a Celite pad, and solvent was removed *in vacuo* from the filtrate. The residue was dissolved in CH_2Cl_2 (*ca.* 4 cm^3) and chromatographed on alumina. Elution with CH_2Cl_2–hexane, initially 2:3 and increasing to 3:2, removed a yellow fraction from the column. Removal of solvent *in vacuo* followed by crystallisation from CH_2Cl_2–hexane (20 cm^3, 1:3) gave yellow *microcrystals* of $[IrAu(CO)(PPh_3)_2(\eta^5\text{-}7,8\text{-}C_2B_9H_9Me_2)]$ **4a** (0.26 g). Crystals suitable for microanalysis were obtained by successive recrystallisations from CH_2Cl_2–hexane (15 cm^3, 1:3) to remove the traces of the slightly less-soluble by-product **5**, followed by crystal growth from a CH_2Cl_2 solution layered with hexane.

(*ii*) The compounds **1a** (0.20 g, 0.27 mmol), *cis*-$[IrCl(CO)_2(NH_2C_6H_4Me\text{-}4)]$ (0.11 g, 0.28 mmol), and $TlBF_4$ (0.15 g, 0.52 mmol) were dissolved in CH_2Cl_2 (20 cm^3) and stirred at room temperature for 6 h. The resulting suspension was filtered through a Celite pad, and solvent removed *in vacuo*. The residue was dissolved in CH_2Cl_2 (*ca.* 3 cm^3) and chromatographed on alumina. Elution with CH_2Cl_2–hexane (1:1) removed an orange fraction, which after removal of solvent *in vacuo* and crystallisation from CH_2Cl_2–hexane (10 cm^3, 1:4) gave pale orange *microcrystals* of $[IrAu(CO)_2(PPh_3)(\eta^5\text{-}7,8\text{-}C_2B_9H_9Me_2)]$ **4c** (0.16 g). Further elution with neat CH_2Cl_2 removed a second, yellow fraction. Solvent was removed *in vacuo* and crystallisation from CH_2Cl_2–Et_2O (10 cm^3, 1:4) at −30 °C gave intense yellow *microcrystals* of $[Ir_2Au_4(\mu\text{-}\sigma\text{:}\eta^5\text{-}7,8\text{-}C_2B_9H_8Me_2)(CO)_3(PPh_3)_4][7,8\text{-}C_2B_9H_{10}Me_2]$ **6** (0.064 g). Crystals suitable for microanalysis were grown from a CH_2Cl_2 solution layered with Et_2O.

(*iii*) A thf (25 cm^3) solution of compound **1a** (0.10 g, 0.13 mmol), $[IrCl(PPh_3)_3]$ (0.14 g, 0.14 mmol), and $TlBF_4$ (0.05 g, 0.17 mmol) was stirred at room temperature for *ca.* 24 h. Solvent was removed *in vacuo* and the residue taken up in CH_2Cl_2 (30 cm^3), which was then filtered through a Celite pad. Solvent was removed *in vacuo*, the material dissolved in CH_2Cl_2 (*ca.* 2 cm^3) and chromatographed on alumina. Elution with CH_2Cl_2–hexane (1:1) removed an orange fraction. Solvent was removed *in vacuo* and crystallisation of the residue from CH_2Cl_2–hexane (10 cm^3, 1:3) gave bright orange *microcrystals* of $[IrAuH(\mu\text{-}\sigma\text{:}\eta^3\text{-}7,8\text{-}C_2B_9H_8Me_2)(PPh_3)_3]$ **8** (0.16 g).

(*iv*) The compounds **1b** (0.11 g, 0.15 mmol), $[IrCl(PPh_3)_3]$ (0.15 g, 0.15 mmol) and $TlBF_4$ (0.06 g, 0.20 mmol) were dissolved in thf (25 cm^3) and stirred at room temperature for 24 h. Solvent was removed *in vacuo* and CH_2Cl_2 (30 cm^3) was added to the residue. The resulting suspension was filtered through a Celite pad, and solvent was then reduced to *ca.* 3 cm^3 *in vacuo*. The solution was chromatographed and elution with CH_2Cl_2–hexane (3:2) removed a broad yellow fraction. Removal of solvent *in vacuo* and crystallisation from CH_2Cl_2–hexane (15 cm^3, 1:3) gave bright yellow *microcrystals* of $[IrAu(PPh_3)_3(\eta^5\text{-}7,8\text{-}C_2B_9H_{11})]$ **9a** (0.15 g).

Synthesis of the Salt $[NEt_4][Ir(CO)_2(\eta^5\text{-}7,8\text{-}C_2B_9H_9$-

Table 7 Crystallographic data[a]

Compound	**4a**	**8**
Crystal dimensions (mm)	0.30 × 0.35 × 0.40	0.20 × 0.22 × 0.23
Molecular formula	$C_{41}H_{45}AuB_9IrOP_2$	$C_{58}H_{60}AuB_9IrP_3$
M	1102.2	1336.5
Crystal colour, shape	Yellow prisms	Dark orange prisms
Crystal system	Monoclinic	Monoclinic
Space group	$P2_1/n$	$P2_1/c$
a/Å	14.922(6)	21.507(4)
b/Å	15.338(7)	12.508(2)
c/Å	18.207(7)	20.669(4)
β/°	94.80(3)	91.24(2)
U/Å^3	4152(3)	5557(2)
Z	4	4
D_c/g cm^{-3}	1.76	1.60
μ(Mo-Kα)/cm^{-1}	68.2	51.4
F(000)	2120	2616
Data collection limits (2θ/°)	5–50	5–40
No. of reflections collected	8192	5815
No. of observed data used	5109	4609
Criterion for data (*n*) used [$F_o \geqslant n\sigma(F_o)$]	5	2
R (R')[b]	0.039 (0.038)	0.032 (0.031)
Final electron-density difference features (maximum, minimum)/e Å^{-3}	1.44, −0.86	0.65, −0.43

[a] Data collected at 293 K on a Siemens R3m/V four-circle diffractometer operating in the Wyckoff ω-scan mode for **4a** and the θ–2θ scan mode for **8**; graphite-monochromated Mo-Kα X-radiation, $\bar{\lambda}$ = 0.710 73 Å. Refinement was by full-matrix least squares with a weighting scheme of the form $w^{-1} = [\sigma^2(F_o) + g|F_o|^2]$ with g = 0.0006 (**4a**) and 0.0013 (**8**); $\sigma^2(F_o)$ is the variance in F_o due to counting statistics; g was chosen so as to minimise variation in $\Sigma w(|F_o| - |F_c|)^2$ with $|F_o|$. [b] $R = \Sigma||F_o| - |F_c||/\Sigma|F_o|$, $R' = \Sigma w^{\frac{1}{2}}||F_o| - |F_c||/\Sigma w^{\frac{1}{2}}|F_o|$.

Table 8 Atomic positional parameters (fractional coordinates × 10^4) for compound **4a**, with estimated standard deviations (e.s.d.s) in parentheses

Atom	*x*	*y*	*z*	Atom	*x*	*y*	*z*
Ir	2740(1)	1629(1)	833(1)	Au	2762(1)	2996(1)	−25(1)
P(1)	2495(2)	810(2)	−227(1)	P(2)	2676(2)	4147(2)	−795(2)
C(1)	2247(7)	901(6)	1867(6)	C(2)	2912(7)	1746(6)	2084(5)
B(3)	2540(9)	2693(8)	1643(7)	B(4)	1511(8)	2410(8)	1091(7)
B(5)	1413(8)	1231(8)	1236(6)	B(6)	2179(9)	1367(9)	2730(7)
B(7)	2360(9)	2493(10)	2581(7)	B(8)	1466(9)	2875(8)	1981(7)
B(9)	761(9)	1986(9)	1730(7)	B(10)	1224(9)	1063(8)	2193(6)
B(11)	1255(8)	2066(8)	2632(7)	C(3)	3964(7)	1635(6)	677(6)
O	4693(5)	1669(5)	595(5)	C(10)	2595(9)	−39(7)	1926(7)
C(20)	3888(7)	1601(8)	2380(6)	C(41)	1505(6)	1023(6)	−864(5)
C(42)	771(7)	1507(8)	−656(6)	C(43)	17(8)	1610(8)	−1149(7)
C(44)	−16(8)	1223(8)	−1840(7)	C(45)	697(8)	757(8)	−2043(6)
C(46)	1443(7)	675(7)	−1557(6)	C(51)	2419(7)	−366(7)	−41(5)
C(52)	3148(9)	−767(7)	325(6)	C(53)	3133(11)	−1659(8)	447(7)
C(54)	2381(14)	−2143(9)	227(8)	C(55)	1641(11)	−1725(8)	−122(8)
C(56)	1651(8)	−851(7)	−253(6)	C(61)	3376(6)	865(6)	−884(5)
C(62)	3930(8)	182(8)	−1017(7)	C(63)	4553(9)	268(9)	−1531(9)
C(64)	4658(9)	1000(9)	−1885(7)	C(65)	4109(10)	1688(9)	−1786(7)
C(66)	3463(9)	1613(8)	−1280(6)	C(71)	2376(7)	3786(6)	−1737(6)
C(72)	2942(9)	3849(9)	−2278(6)	C(73)	2762(11)	3477(9)	−2962(7)
C(74)	1961(10)	3066(9)	−3124(8)	C(75)	1375(9)	2982(10)	−2571(8)
C(76)	1584(8)	3349(8)	−1900(8)	C(81)	3698(7)	4780(7)	−848(5)
C(82)	4489(8)	4342(9)	−896(6)	C(83)	5289(9)	4794(13)	−969(7)
C(84)	5272(11)	5690(14)	−973(7)	C(85)	4492(12)	6127(11)	−913(8)
C(86)	3689(9)	5684(8)	−859(7)	C(91)	1825(7)	4924(7)	−568(7)
C(92)	1653(8)	5019(7)	156(7)	C(93)	1019(9)	5597(9)	370(8)
C(94)	568(9)	6101(10)	−159(11)	C(95)	703(10)	6022(9)	−861(12)
C(96)	1335(8)	5430(8)	−1091(8)				

Table 9 Atomic positional parameters (fractional coordinates × 10^4) for compound **8**, with e.s.d.s in parentheses

Atom	*x*	*y*	*z*	Atom	*x*	*y*	*z*
Ir	2962(1)	5142(1)	2097(1)	Au	1778(1)	5455(1)	2520(1)
P(1)	3311(1)	4610(2)	3104(1)	P(2)	3338(1)	6856(2)	2078(1)
P(3)	916(1)	5919(2)	3114(1)	C(1)	2971(4)	3298(6)	1023(4)
C(2)	3046(4)	4327(7)	653(4)	C(10)	3534(5)	2573(8)	1130(5)
C(20)	3662(5)	4605(8)	374(5)	B(3)	2643(5)	5358(8)	1020(5)
B(4)	2154(5)	4778(7)	1628(5)	B(5)	2519(5)	3488(9)	1687(5)
B(6)	2600(6)	3338(9)	284(5)	B(7)	2384(5)	4697(8)	272(5)
B(8)	1823(5)	4924(9)	866(5)	B(9)	1731(5)	3705(8)	1288(5)
B(10)	2253(5)	2785(9)	961(5)	B(11)	1830(6)	3701(9)	454(5)
C(32)	2598(2)	2828(5)	3354(3)	C(33)	2476	1739	3419
C(34)	2955	997	3357	C(35)	3556	1345	3229
C(36)	3678	2435	3164	C(31)	3199	3176	3226
C(42)	4578(3)	4548(4)	2842(2)	C(43)	5211	4712	2968
C(44)	5410	5144	3559	C(45)	4976	5412	4025
C(46)	4344	5248	3899	C(41)	4144	4816	3308
C(52)	2651(3)	6112(4)	3811(2)	C(53)	2420	6566	4373
C(54)	2480	6024	4961	C(55)	2772	5028	4987
C(56)	3003	4574	4424	C(51)	2943	5116	3836
C(62)	4449(3)	6417(5)	1444(3)	C(63)	4887	6542	962
C(64)	4782	7277	463	C(65)	4239	7886	447
C(66)	3801	7761	929	C(61)	3906	7026	1427
C(72)	4390(3)	7418(5)	2870(3)	C(73)	4679	7892	3408
C(74)	4325	8427	3863	C(75)	3680	8488	3781
C(76)	3390	8014	3243	C(71)	3745	7479	2788
C(82)	2939(2)	9001(5)	1975(3)	C(83)	2510	9818	1852
C(84)	1905	9569	1648	C(85)	1728	8503	1566
C(86)	2157	7687	1688	C(81)	2762	7936	1892
C(92)	1300(3)	8006(6)	3250(2)	C(93)	1392	8973	3575
C(94)	1194	9088	4210	C(95)	905	8237	4519
C(96)	814	7271	4194	C(91)	1011	7155	3559
C(102)	−235(3)	6834(6)	2757(3)	C(103)	−702	7093	2305
C(104)	−677	6697	1676	C(105)	−185	6042	1497
C(106)	282	5782	1949	C(101)	257	6178	2579
C(112)	87(3)	4608(6)	3807(3)	C(113)	−39	3878	4297
C(114)	443	3486	4692	C(115)	1052	3825	4597
C(116)	1179	4556	4107	C(111)	697	4947	3712

Me_2)].—A thf (20 cm^3) solution of *cis*-[$IrCl(CO)_2(NH_2C_6H_4$-Me-4)] (0.11 g, 0.28 mmol) was treated with Tl[Tl-$C_2B_9H_9Me_2$] (0.16 g, 0.28 mmol), and the mixture was stirred at room temperature for 1 h. The salt [NEt_4]Cl (0.06 g, 0.28 mmol) was added and the reactants stirred for 1 h. Solvent was then removed *in vacuo*, CH_2Cl_2 (30 cm^3) added, and the resulting suspension filtered through a Celite pad. Solvent was removed *in vacuo* and oily brown *microcrystals* of [NEt_4][$Ir(CO)_2$-(η^5-7,8-$C_2B_9H_9Me_2$)] **7** (0.09 g) were formed by crystallisation from CH_2Cl_2–Et_2O (10 cm^3, 1:3) at −30 °C. Crystals suitable for microanalysis were obtained by chromatographing the crude material (2 × 10 cm alumina column). Elution with neat CH_2Cl_2 removed a yellow fraction, from which solvent was removed *in vacuo*. Pale brown *microcrystals* of **7** were grown by diffusion of Et_2O into a layer of a CH_2Cl_2 solution of the material.

Synthesis of the Complex [$IrAu(CO)_2(PPh_3)(\eta^5$-7,8-$C_2B_9H_9$-Me_2)].—The compounds **7** (0.11 g, 0.20 mmol), [$AuCl(PPh_3)$] (0.10 g, 0.20 mmol) and $TlBF_4$ (0.07 g, 0.24 mmol) were dissolved in CH_2Cl_2 (20 cm^3) and stirred at room temperature for 1.5 h. The resulting suspension was filtered through a Celite pad and solvent removed *in vacuo*. The residue was dissolved in CH_2Cl_2 (*ca.* 2 cm^3), chromatographed on alumina and an orange fraction was eluted with CH_2Cl_2–hexane (1:1). Solvent was removed *in vacuo* and pale orange *microcrystals* of [$IrAu(CO)_2(PPh_3)(\eta^5$-7,8-$C_2B_9H_9Me_2$)] **4c** (0.11 g) were crystallised from CH_2Cl_2–hexane (10 cm^3, 1:4).

Crystal Structure Determinations and Refinements.—The crystal data and experimental parameters for compounds **4a** and **8** are given in Table 7. Crystals of both **4a** and **8** were grown by the method of diffusion of hexane into CH_2Cl_2 solutions of the compounds. The selected crystals were mounted in sealed glass capillaries under nitrogen. All data were corrected for Lorentz, polarisation and X-ray absorption effects, the latter by an empirical method based upon azimuthal scan data.[14]

For compound **4a** all non-hydrogen atoms were refined with anisotropic thermal parameters. The cage B–H hydrogen atoms were located in a final electron-density difference synthesis, and their positions were refined with fixed isotropic thermal parameters (U_{iso} = 0.08 $Å^2$). Methyl and phenyl hydrogen atoms were included in calculated positions (C–H 0.96 Å) with fixed isotropic thermal parameters (U_{iso} = 0.08 $Å^2$).

For compound **8** all non-hydrogen atoms were refined with anisotropic thermal parameters and the phenyl rings were included as rigid groups. The terminal Ir–H(001) hydride and the cage B–H hydrogen atoms were located in final electron-density difference maps and their positions were refined with fixed isotropic thermal parameters (U_{iso} = 0.08 $Å^2$). Methyl and phenyl hydrogen atoms were included in calculated positions (C–H 0.96 Å) with fixed isotropic thermal parameters (U_{iso} = 0.08 $Å^2$). All computations were performed on a DEC μ-Vax II computer with the SHELXTL system of programs.[14] Scattering factors with corrections for anomalous dispersion were taken from ref. 15 and atomic coordinates are listed in Tables 8 and 9.

Additional material available from the Cambridge Crystallographic Data Centre comprises H-atom coordinates, thermal parameters, and remaining bond lengths and angles.

Acknowledgements

We thank the SERC for a research studentship (to P. A. J.), and the Robert A. Welch Foundation for support (to P. A. J. and F. G. A. S.).

References

1 J. C. Jeffery, P. A. Jelliss and F. G. A. Stone, preceding paper.
2 A. L. Casalnuovo, J. A. Casalnuovo, P. V. Nilsson and L. H. Pignolet, *Inorg. Chem.*, 1985, **24**, 2554 and refs. therein.
3 H. Lehner, D. Matt, P. S. Pregosin, L. M. Venanzi and A. Albinati, *J. Am. Chem. Soc.*, 1982, **104**, 6825.
4 (*a*) M. U. Pilotti, F. G. A. Stone and I. Topaloğlu, *J. Chem. Soc., Dalton Trans.*, 1991, 1355; (*b*) N. Carr, M. C. Gimeno, J. E. Goldberg, M. U. Pilotti, F. G. A. Stone and I. Topaloğlu, *J. Chem. Soc., Dalton Trans.*, 1990, 2253.
5 J. C. Jeffery, P. A. Jelliss and F. G. A. Stone, unpublished work.
6 J. C. Jeffery, M. A. Ruiz, P. Sherwood and F. G. A. Stone, *J. Chem. Soc., Dalton Trans.*, 1989, 1845.
7 M. I. Forsyth, D. M. P. Mingos and A. J. Welch, *J. Chem. Soc., Dalton Trans.*, 1978, 1363.
8 N. N. Greenwood, J. D. Kennedy and D. Reed, *J. Chem. Soc., Dalton Trans.*, 1980, 196; J. D. Kennedy, *Prog. Inorg. Chem.*, 1984, **32**, 519.
9 E. J. M. Hamilton and A. J. Welch, *Polyhedron*, 1990, **9**, 2407.
10 J. P. Collman, C. T. Sears, jun., and M. Kubota, *Inorg. Synth.*, 1968, **11**, 101.
11 U. Klabunde, *Inorg. Synth.*, 1974, **15**, 82.
12 R. Usón and A. Laguna, *Organomet. Synth.*, 1986, **3**, 325.
13 M. A. Bennett and D. L. Milner, *J. Am. Chem. Soc.*, 1969, **91**, 6983.
14 G. M. Sheldrick, SHELXTL programs for use with a Siemens X-Ray System, Cambridge, 1976; updated Göttingen, 1981.
15 *International Tables for X-Ray Crystallography*, Kynoch Press, Birmingham, 1974, vol. 4.

Received 23*rd September* 1992; *Paper* 2/05109E